The curled pointy & straight terminals of α-synuclein
A calorimetric study of α-synuclein fibril formation & peptide induced vesicle leakage
KEML13

Emil Axell

May 31, 2017

A thesis presented for the degree of
Bachelor of Science

LUND UNIVERSITY
Faculty of Science

Center for Molecular Protein Science

Date performed: Spring 2017
Supervisor: Martin Lundquist

1 Abstract

The small protein α-synuclein is strongly associated with Parkinson's disease. This protein is found in inclusion bodies, named lewy bodies inside neurons of people suffering from the disease. α-synuclein is very abundant in the human brain, and its normal function is still elusive and unclear. The factors that trigger the accumulation and fibrillation of this protein into pathogenic inclusion bodies is of great interest in the quest of finding a cure for the disease. In this study the isothermal fibrillation of this protein from monomeric form (found in the brain of healthy people) into aggregated structures (found in people with the disease) was investigated using calorimetry. This yielded insights about the underlying thermodynamics that govern the onset and progression of the disease. This work shows that the process of fibrillation is endothermic (needs energy to proceed) under the investigated conditions and that calorimetry is a method that may be employed in the study of this protein. Attempts were made to investigate whether this protein had an effect on proton permeability across the membrane of small unilamellar vesicles, with a pH gradient between the interior and exterior of the vesicles. In doing so groundwork was laid for developing a vesicle leakage assay using the lytic peptide melittin and studying leakage through isothermal titration calorimetry.

Contents

2 Introduction

Throughout the last decades, human life expectancy has increased dramatically[1]. During this time of rapid prolongation of our lifespan, the landscape of the top causes of human death has shifted. Emerging among these top causes are neurodegenerative diseases. In developed countries, Alzheimer's disease and Parkinson disease (PD) are now among the top 6 and 15, respectively, leading causes of death[2, 3]. Along with an increasing elderly population, the number of people suffering from neurodegenerative diseases is likely to continue to grow[4, 5]. More knowledge surrounding the pathogenesis of these diseases is required to be able to design and develop new treatments that could stall or completely prevent their fatal courses. Multiple neurodegenerative diseases is associated with protein misfolding[6]. The main mischief makers of Alzheimer's disease and PD are thought to be the proteins Amyloid beta and Alpha synuclein (α-syn). There are many similarities between the two diseases, but to narrow down the scope, this thesis will devote attention towards α-syn.

α-syn is a small protein consisting of 140 amino acids [7]. In solution it is considered to be intrinsically disordered [8], meaning it lacks one single stable 3-D configuration. α-syn is highly abundant in the human brain where it makes up 1% of the cytosolic proteins in neurons [9, 10]. The normal function of α-syn is elusive and still not well understood.

The N-terminal of α-syn (residues 1-60) include repeats of amphipathic character, which in turn may anchor α-syn to membranes [11]. This is possible because of the amphipathic nature of lipids themselves. The hydrophobic/hydrophilic parts of the protein has affinity towards the hydrophobic/hydrophilic parts of the lipids making up the membrane. Electrostatic interactions are also important for the binding. The associated entropy gain of water from burying hydrophobic parts of the protein in the hydrophobic parts of the membranes is also a driving force for binding. In association with membranes, the N-terminal of α-syn adopts a highly α-helical structure [11]. The amphipathic repeats in the N-terminal of α-syn, bear resemblance to the lipid-binding domain of apolipoproteins. With especially close similarity to the subclass A2 amphipathic alpha helices [12]. This resemblance is something that provides further clues as to why α-syn has affinity towards membranes. Several studies has shown that α-syn has a higher affinity towards membranes containing lipids with negatively charged head groups, and in many cases does not associate, at all, with vesicles containing only zwitterionic lipids [13, 14].

Several functions of α-syn may lie in the synaptic terminals, a compartment at the end of the axon, containing neurotransmitters (small molecules eg. dopamine encapsulated in small vesicles), crucial for signal propagation between neurons in the brain. There, in the synaptic terminals, it has been suggested that α-syn is involved in moderation of synaptic vesicle supply [15] in release of chemical messengers [16] and the fusing of vesicles at the synapse [17]. The interaction

of α-syn and model lipid membranes is well established, but the implications of these interactions is not fully understood.

The aggregation of monomeric α-syn into insoluble amyloid fibrils is a process that is thought to be the key element of PD onset and progression. Which factors that triggers and accelerate this onset and progression is something that has been studied excessively *in vitro*. The aggregation of α -syn is a nucleation dependent process [18], which means that pre formed seeds may trigger and accelerate the process of aggregation. α-syn fibrillation involves multiple secondary processes like fragmentation of fibrils.

Solution conditions has been shown to have an effect on the different rate constants governing the kinetics of aggregation. At mildly acidic pH, the rate of aggregation is much more rapid than at physiological pH. It has also been shown that fibrils grow by monomer, not by oligomer addition [19]. Solution conditions also have an effect on the sign of enthalpy associated with monomer binding to fibril seeds. At pH 7.4 the enthalpy of fibril elongation by monomer is accompanied by heat absorption, at pH 2.5, the sign of enthalpy is reversed[20].

Various experimental techniques is employed to study the process of protein aggregation. A few among the most readily used consist of different types of spectroscopy, like circular dichroism and time-resolved fluorescence (with the use of dyes that undergoes spectroscopic shifts upon interaction with amyloid species). Other methods include different NMR-experiments and more morphological experiments may relay on atomic force microscopy and different scattering techniques. Each of the techniques have their advantages and disadvantages. Everyone of them applied *in vitro* in the quest of better understanding the processes happening *in vivo*.

Calorimetric techniques have the power to elucidate many of the underlying thermodynamic parameters that governs the onset and progression of protein mis-folding. In the literature, there exist a substantial body were different calorimetric techniques are employed to study different characteristics of amyloid species[21, 22, 23], but only a few concerning α-syn in particular [20].
These studies often focus on the heat of denaturation of already formed aggregates, or the enthalpy of heat induced aggregation in thermal up/down scans in differential scanning calorimeters. Limited studies investigate the accompanied enthalpy change of the self assembly of monomeric species into fibrils, isothermally[24]. It has been shown that the enthalpy change associated with aggregation of β_2-microglobulin is detectable through ITC[25], without performing any injections during the aggregation stage, merely by monitoring the process isothermally.

This work intend to show that the process of α-syn aggregation is a process that is detectable through isothermal calorimetry, by monitoring the fibril formation from monomeric species isothermally.

3 Experimental Method

3.1 Protein purification & seed fibril formation

3.1.1 Purification of α-syn monomer

Human wild type α-syn expressed in *E.coli* following the procedure described in [26], was acquired in the lab and stored at -20 °C during the duration of the work.

When monomer was used, the α-syn from the freezer was always further purified by size exclusion chromatography (SEC) through a Superdex 75 or a Superdex 75 increase column (GE Healthcare), using the experimental buffer 10 mM MES pH 5.5. For the experiments where a higher concentration α-syn monomer was used, multiple tubes of protein was first lyophilized and then dissolved in 6 M Guanidine hydrochloride, 10 mM MES pH 5.5, before being run through the SEC column using the experimental buffer. The eluted monomers were collected in low binding protein tubes and strictly kept on ice before the aggregation experiments were initiated.

The protein concentrations were determined by measuring absorbance at 280 nm with a NanoDrop 2000 (Thermo scientific) and calculated with Beer Lambert's law using an extinction coefficient of 5120 $M^{-1}cm^{-1}$. (Each monomer solution was measured a total of 9 times, 2 μL was loaded on the NanoDrop and meassured 3 times, this process was repeated another 2 times.)

3.1.2 α-syn seed fibril formation

α-syn seed fibrils were prepared by letting α-syn monomer of known concentration, purified through SEC, aggregate in low binding eppendorf tubes under moderate stirring with a small magnetic bar. The monomers were left to fibrillate for $\approx$ 48h in a 37 °C incubator, upon which after, insoluble fibril aggregates were visible in the tube. The tube containing the aggregated α-syn was then placed in a sonication bath (Struer) and sonicated for one minute. The seeds were frozen in aliquots and stored at -20 °C until needed.

3.2 Vesicle preparation & size determination

3.2.1 Lipid preparation

Lyophilized lipids were purchased from Avanti Polar lipids®. 5 mM stock solutions of the different lipids were prepared through dissolving the lipids in Chloroform:Methanol (9:1), to obtain a homogeneous distribution of lipids in solution. Additional stock solutions of lipids with various lipid compositions, diverse working buffers and with individual pH was made through mixing aliquots of lipids from the Chloroform:Methanol stock's in glass test tubes at desired lipid ratios. The solvent was evaporated under dry nitrogen steam in a fume hood

and the tube was left in a vacuum dessicator over night to remove any trace of remaining solvent. The formed lipid film was then rehydrated in the preferred buffer and freeze thawed in 10 cycles (frozen in a dry ice/ethanol bath and melted in 37 °C incubator under vigorous shaking). All stock solutions were stored at -20 °C, during the duration of the work.

3.2.2 Vesicle preparation

SUV's were prepared through sonication. 1 ml lipid suspensions, contained in either small glass vials or eppendorf tubes were sonicated for 14 minutes, 1 second on, one second off at maximum amplitude of 8, in a soniprep 150 plus (MSE), equipped with an exponential probe. The glass vials/eppendrof tubes were submerged in an ice bath during sonication. After sonication, the solution was centrifuged at 8161 RCF for 3 minutes (Biofuge 13, Baxter Heraeus), to sediment any potential titanium debris from the sonicator probe and the vesicle solution was transferred to a new eppendorf tube.

To obtain a pH gradient between the interior and exterior of the SUV's, a calibrated amount of 1M HCl, from pure buffer, were added to the lipid suspensions. To obtain this calibrated amount, 1M HCl was titrated into 20 mL 50 mM Tris pH 9. HCl was added until the pH was lowered to 7.4. The amount HCl required to lower the 20 mL solution form 9 -> 7.4, was divided by 10 and added to 2 mL solution containing the vesicles prepared in 50 mM Tris pH 9. This procedure was also carried out for vesicles prepared in 10 mM MES pH 6.7, in that case 1M HCl was added to lower the pH to 5.5. The influence of the vesicles themselves, on the pH were not accounted for.

3.2.3 Size determination of vesicles

The size of the SUV's were determined through nano tracking analysis (NTA) with a Nanosight LM10, (Malvern instruments). This method yields both size and concentration distribution of vesicles in suspension. These characteristics are obtained by sending a laser beam through the vesicle suspension. Subsequently, vesicles in the path of the laser beam scatter light. The scattered light is then visualized in a microscope. The movement/diffusion of vesicles, due to Brownian motion, is recorded with a camera mounted on the microscope. From this recording, a software tracks individual vesicles movement, and through the Stokes-Einstein relation, calculates the vesicles hydrodynamic radius.

When SUV's are prepared through freeze thawing and sonication, the vesicles will be polydisperse, meaning there might even be large unilamellar vesicles present in the solution. Larger vesicles could introduce bias in the size determination, because they scatter more light than smaller vesicles. This risk is fairly low because the vesicle suspensions were significantly diluted prior to analysis to reduce the number of particles. The LM10 requires samples with a concentration ranging from 10^6 to 10^9 particles per mL, to able to distinguish and

accurately track, individual particles.

3.3 Calorimetry

Calorimetric measurement was performed in a VP-ITC,VP-DSC and Peaq-ITC (Malvern instruments). All samples used in the VP instruments were degassed under stirring and thermostatted to $\approx$ 25 °C for 10 minutes in a Thermovac (Microcal), before being loaded in the sample cells (or the injection syringe of the ITC). For the seeded/vesicle induced aggregation experiments of α-syn, the monomer was first degassed for approx 5 minutes before the vesicles/seeds were mixed in with the monomers and degassed for another 5 minutes.

For further information about cell loading and general operation of the instruments, consult the user manual of the three calorimeters[ABC].

3.3.1 Isothermal titration calorimetry

Isothermal titration calorimetry (ITC) is a widely used technique to characterize the thermodynamics parameters of binding between two (or more) species in solution, eg. protein-ligand. The main components of an ITC is a sample and reference cell and an injection syringe. The sample and reference cell is separated by a peltier element to have maximum heat conductivity between the cells. During the measurement a small current is supplied to the reference and sample cell heaters, to maintain the cells at a constant temperature and ΔT=0 between the cells. Known amounts of ligand is injected into the sample cell containing the protein. The resulting enthalpy change associated with binding of the ligand to the protein is then detected as a power differential (DP) needed to maintain the sample and reference at the same temperature. Depending on the sign of enthalpy of binding between protein in ligand, the DP will either deflect in positive or negative direction. When the heat, either absorbed or evolved in the sample cell has equilibrated with the reference cell, the DP will return to the baseline. The DP is converted and reported as μCal/s. When the resulting peak from an injection is integrated with respect to time and normalized with respect to the number of moles ligand injected, the molar enthalpy of binding is obtained. As the binding sites on the protein in the sample cells gets saturated with ligand, the enthalpy of binding decreases gradually with each new injection, until the protein is fully saturated and the observed ΔDP is only due to the enthalpy of dilution of the ligand. From the corresponding thermogram the enthalpy (from the normalized integrated peak of the first injection when all injected ligand binds to the protein), binding affinity (from the slope of the decreasing DP signal) and stoichiometry (from the midpoint of the slope

[A] http://www.malvern.com/Assets/MicroCal-VP-DSC-system-operating-instructions-English-MAN0568-01-EN-00.pdf

[B] http://www.malvern.com/Assets/MicroCal-VP-ITC-system-operating-instructions-English-MAN0569-01-EN-00.pdf

[C] http://www.malvern.com/Assets/MicroCal-PEAQ-ITC-user-manual-English-MAN0573-02-EN-00.pdf

if binding is 1:1) of the binding reaction is obtained, subsequently the entropy and Gibbs energy of the reaction is also obtained.

When performing ITC a buffer with a low ionization enthalpy is preferred, this to reduce the effects of buffer mismatch. Normally the same buffer is used for the solute in the syringe and in the sample cell. If these buffers have slightly different pH, the enthalpy change of the corresponding ionization of the buffer, following injection will affect the observed enthalpy change associated with binding. Often dialysis is performed on both the species, to ensure that the buffers they are dissolved in have the exact same pH. This reduces the potential of the enthalpy change corresponding from injection of a buffer with one pH into a buffer with a different pH. If there is a buffer mismatch between the buffer used in the syringe and the one used in the sample cell, the ionization enthalpy have the potential to transcend the enthalpy change of binding when performing ITC.

In this work the capabilities of ITC is exploited, not to observe binding of ligand to macromolecule, but rather to investigate whether ITC may be used to detect the permeability of protons across the lipid bilayer of vesicles. In doing so, a buffer with a high ionization enthalpy is working in the advantage of the experimental design.

This was done by injecting the peptide melittin (which is known to cause membrane permeability) into the sample cell containing SUV's with a pH gradient between the interior of the vesicles and the exterior bulk solution.

The enthalpy change of α-syn fibrillation was also monitored in the ITC. Both by injecting an aliquot of preformed α-syn seeds into the cell containing α-syn monomer and by having seeds/monomer premixed in the sample cell.

The experimental procedures differed slightly between those experiments performed in the VP-ITC and those in the PEAQ-ITC. The VP-ITC has a maximum time spacing between each injection of $\approx$ 24h, while in the PEAQ-ITC only $\approx$ 2.8h. The injection of seeds was usually performed after an initial delay, followed by the maximum time spacing for the different instrument. Consult each figure text for further details.

The peaks corresponding from injections were integrated and analyzed in Origin 7.0 for those experiments performed in the VP-ITC and MicroCal PEAQ-ITC analysis software for the experiments conducted in the PEAQ-ITC.

3.3.2 Differential scanning calorimetry

Differential scanning calorimetry (DSC) is a technique that may be used to study the enthalpy and heat capacity change accompanying a wide range of thermal transition of species in solution, e.g. it may be used to study the thermal stability of biomolecules when heated, or the cold denaturation of proteins.

The arrangement of the instrument is similar to the ITC, where the DP between the sample cell and reference is reported to the user. But instead of measuring the accompanied change in DP from an injection, the DSC measures the change in DP upon heating/cooling both the cells. In a typical protein denaturation experiment, the protein is loaded in the sample cell and the experiment buffer is loaded in the reference cell. A constant power is supplied to heat both cells in a synchronized manner. When the cells reaches the temperature of transition, e.g. where the protein starts to unfold. The energy needed to maintain the cells at same temperature will start to differentiate as a consequence of the change in heat capacity and the associated enthalpy change of the protein as it unfolds.

During this work, only isothermal scans at 37 °C was performed in the DSC.

4 Results

4.1 Fibrillation of α-syn

The process of α-syn fibrillation was monitored isothermally through calorimetry, in a VP-DSC, VP-ITC and a PEAQ-ITC. This was done to investigate the thermodynamic properties associated with the self assembly of monomeric α-syn into aggregated fibrillar structures. Performing these scans isothermally yields insight about the enthalpy change accompanying this process. The concentration of α-syn monomer and seeds used, were varied throughout the different scans. Depending on which instrument that was used, the seeds and monomer were either pre mixed or the seeds were injected into the cell containing the monomer, once the scan had begun. Figure 1 (a-d) shows the change in DP over time for the process occurring when monomer was incubated with seeds in a DSC. After the scans, the samples were collected in eppendorf tubes and insoluble aggregates was visible in all 5 experiments. The reason for only performing one 16 hour scan in figure 1(c) was to confirm that fibrils were visible after the peak between 200 & 600 min had occurred. The same monomer/seed solution used in figure 1(b), was also scanned in a PEAQ-ITC see figure 11(b) in appendix 1. The scan performed in the PEAQ-ITC did not display the same characteristics, with a clear peak as seen in the scans performed in the DSC.

Figure 2 and in appendix 1; figure 11(a) & 12(e)-(f), shows the isothermal scan of monomer incubated with different vesicles, with and without a pH gradient between the interior and exterior of the vesicles. Figure 3 & 4 and in appendix 1; figure 10, 13 and 14 shows the isothermal scans of α-syn monomer incubated with and without seeds.

Consult each individual figure caption for a more in depth review of the different experiment parameters.

4.1.1 Monitored in VP-DSC

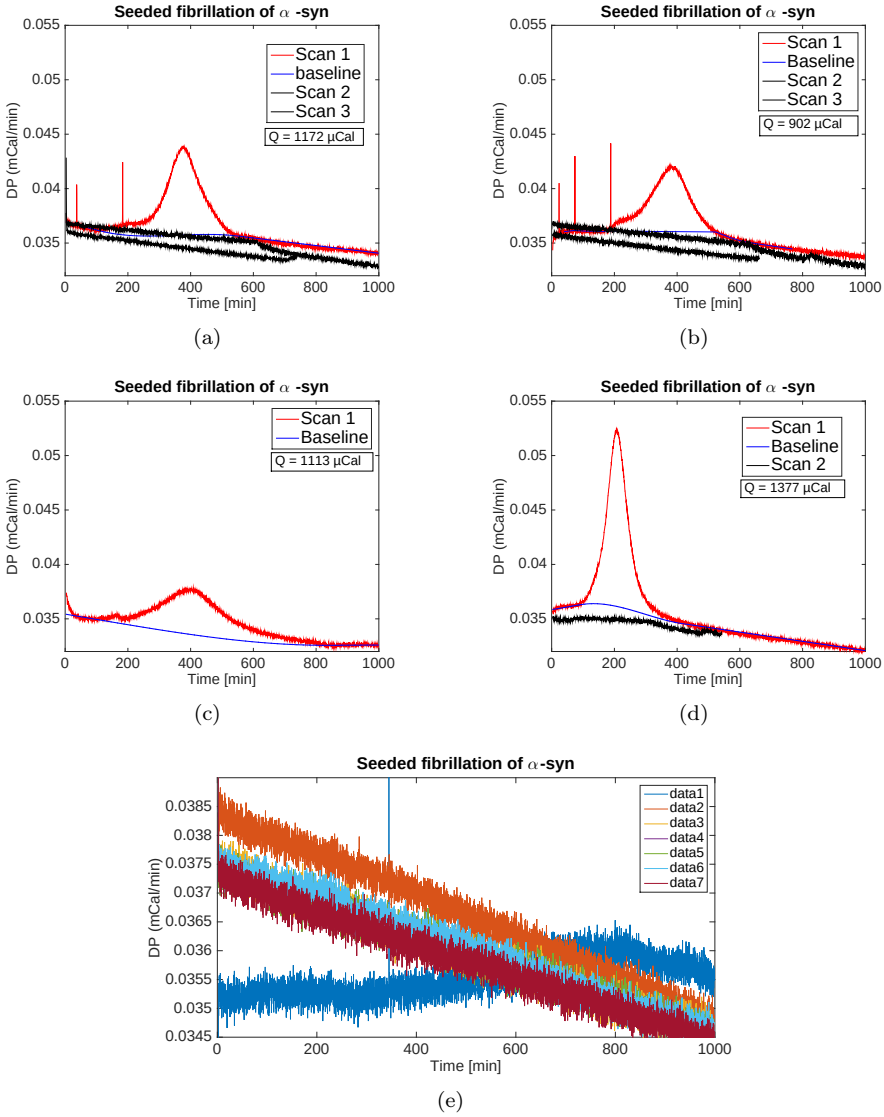

Figure 1: (a-d) Shows isothermal scans of the seed induced fibrillation of α-syn. In the sample cell: 134 μM α-syn monomer, 2 μM seeds, in 10 mM MES, 0.01% NaN_3 pH 5.5. Pure buffer was used in the reference cell. The scans were performed at 37°C, 27±1 Psi, low feedback mode, with a filtering period of 25 s. The baselines were fitted locally through a baseline session in Origin 7.0. The peaks were integrated and the integrals are displayed as Q in each graph. The monomer used in each set of scans (a-e), was purified separately, just prior to each scan. The only thing different in (e) is that a filtering period of 5 s was used.

4.1.2 Monitored in VP-ITC

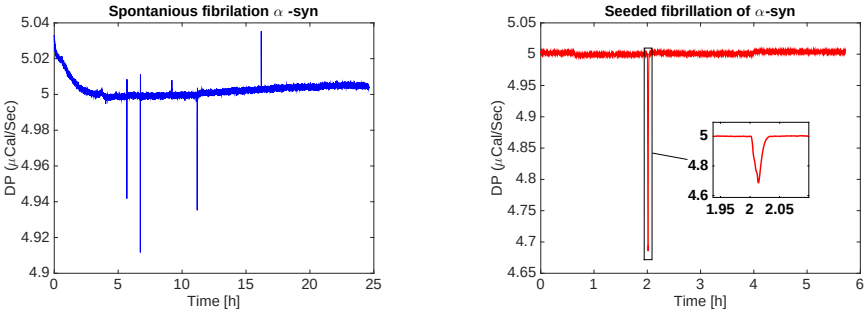

(a) (b)

Figure 2: (a) shows the isothermal scan of 39 μM α-syn monomer incubated at 37°C in 10 mM MES, 0.01% NaN_3, pH 5.5. The syringe was loaded with buffer and a 1 μL injection was performed after 24h. The scan was stopped and the syringe reloaded with 36 μM seeds. The scan was started again (b), after a 2h initial delay 40 μL seeds were injected in the same monomer solution as in (a), to a final cell seed concentration of 1 μM. The corresponding injection peak is magnified and displayed as a subplot in (b).

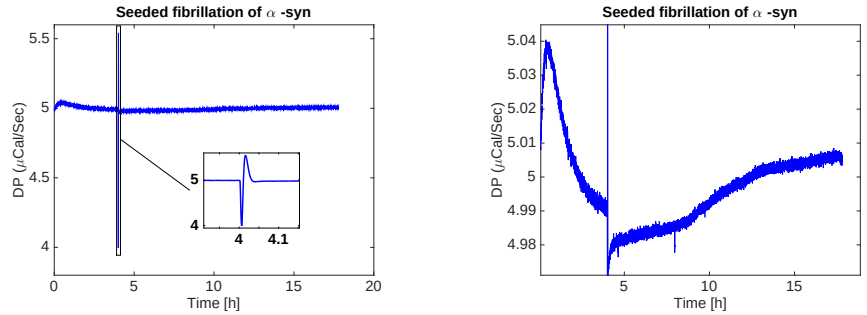

(a) (b) A zoom in of (a)

Figure 3: Shows the isothermal scan of 26 μM α-syn monomer incubated at 37 °C and the injection of 40 μL 36 μM seeds to a final cell seed concentration of 1 μM. Figure (a) contains a subplot of the corresponding injection peak and (b) is a zoom in of the scan.

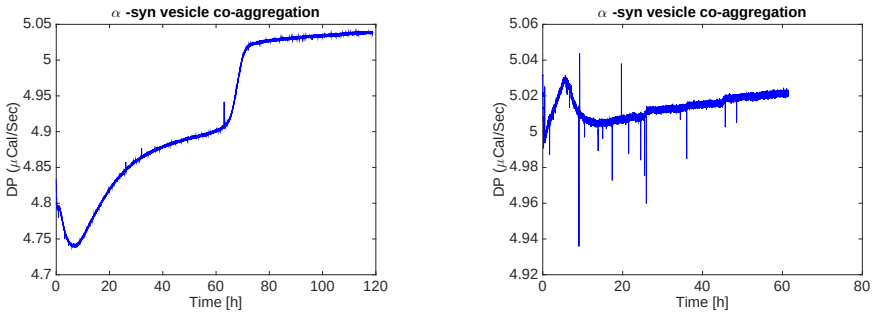

(a) (b)

Figure 4: (a)&(b) shows the isothermal scans, performed at 37 °C. In the sample cell: 24 μM α-syn monomer incubated with 0.17 mM sonicated DOPC:GM1(9:1), in 10 mM MES, 0.01% NaN_3, pH 5.5. The syringe was loaded with 10 mM MES, 0.01% NaN_3, pH 5.5, 1 μL injections was performed every 24h. A temperature drift had occurred in scan (a) and the temperature was 38.4 °C when the scan was stopped after $\approx$ 120h. The monomer and vesicles used in (a)&(b) was purified and prepared separately.

4.2 Vesicle leakage

4.2.1 Melittin induced vesicle leakage

The concentration of melittin injected into the vesicle solutions was varied throughout these experiments. The vesicle concentration was also changed back and fourth, in an attempt to find a ratio between vesicle and melittin where complete leakage of the vesicles internal solution could be observed. Many of the different ratios was investigated both with a pH gradient between the interior and exterior of the vesicles, but also with the same pH inside and outside. In the plot legends where only Tris is annotated, corresponds to 50 mM Tris, 0.2% EDTA, 0.02% NaN_3 pH 7.4. This is the working buffer for all experiments performed with melittin.

Figure 5 show the corresponding change in DP from injecting 75 μM melittin into different concentrations DOPC:DOPS (3:1), with and without pH gradient. Figure 6(a)&(b) show the size distribution of the vesicles before and after injection of melittin of two of the injection series in figure 5.
Figure 7(a) & (b) show injections of different concentrations of melittin into 1.5 mM DOPC:DOPS (3:1), with a pH gradient between the interior and exterior of vesicles in (a) and the same pH inside and outside in vesicles in (b). Figure 8 show the size distribution before and after injection of melittin in the vesicles used in 7(a). Table 1 show the integrated peaks of the injections carried out in figure 7(a).

Additional experiments where melittin were injected into vesicles may be found in appendix 2; Figure 15(a), show injection of decreasing concentrations melittin (100μL, 50μL, 25μL, 10μL) in 1.5 mM DOPC:DOPS (3:1) with a pH gradient. Figure 16 show the injection of 0.3 mM melittin into 0.5 mM vesicle solution.

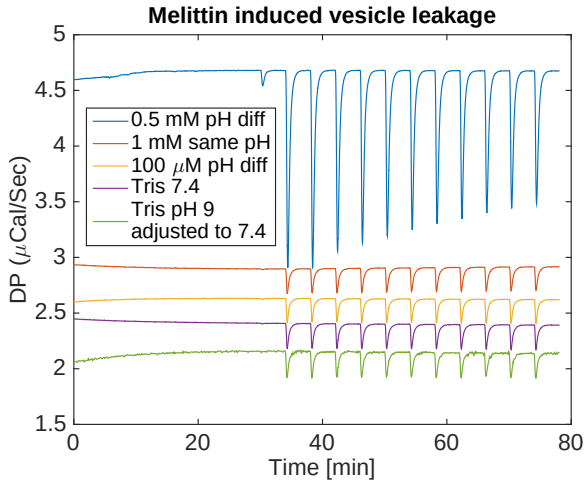

Figure 5: Show the corresponding change in DP from injecting the same volume, 25 μL, 75 μM melittin into: In blue; 0.5 mM vesicles with pH gradient. In orange; 1 mM vesicles no gradient. In yellow; 0.1 mM vesicles with pH gradient. In purple; Tris pH 7.4. In green; Tris adjusted from pH 9 to 7.4 in the same way as the gradient in the vesicle solutions. All vesicles used were DOPC:DOPS (9:1), the experiments were performed at 37 °C with 307 RPM stirring in a VP-ITC. An offset in y-direction, has been added to each dataset for better visualization of the peaks.

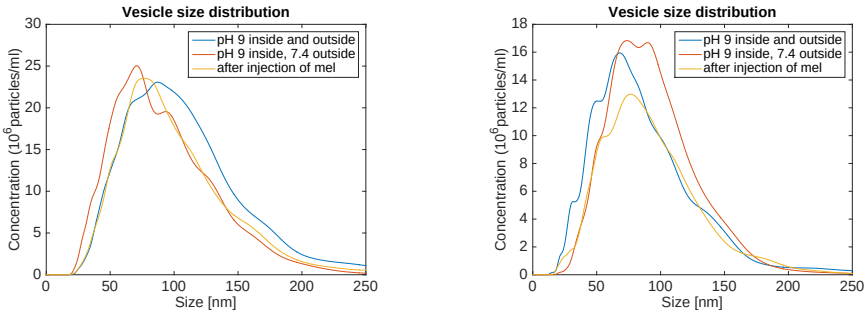

(a) (b)

Figure 6: Show the size distribution of vesicles before adjusting pH outside of vesicles to 7.4, after adjusting pH and after injecting melittin into vesicles. The vesicles investigated is the ones used in figure 5. (a) show the size of vesicles before and after injection of melittin in the same vesicles as those used in the blue curve of figure 5. (b) show the vesicles used in yellow curve of figure 5. The vesicles were diluted to 1.5 μM before NTA was performed.

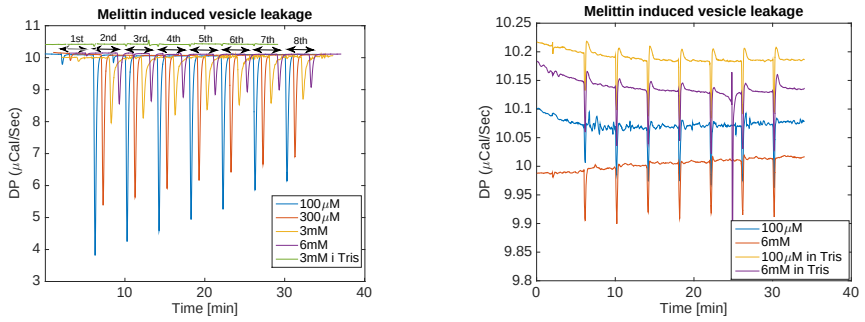

(a) pH 9 inside, 7.4 outside vesicles. (b) pH 7.4 inside and outside vesicles.

Figure 7: Show the corresponding change in DP from injecting the same volume, 5μL melittin of different concentrations, into a constant concentration of 1.5 mM DOPC:DOPS (3:1). The vesicles used in (a) has a pH gradient, pH 9 inside, 7.4 outisde. The vesicles in (b) has the same pH, 7.4 inside and outside. The experiments were performed at 37°C, 500 RPM stirring in a PEAQ-ITC. A phase shift has been added to the data in (a), (Time of first injection + n minutes (n=0,1,2,3). The data for injection of melittin in Tris has rather been added an vertical offset, for better visualization.

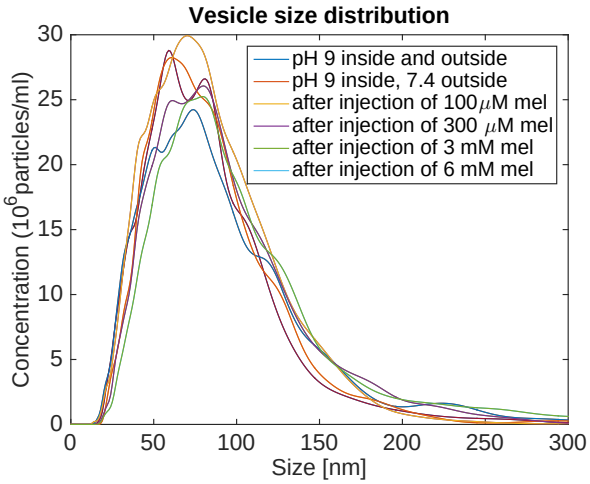

Figure 8: Show the size distribution of vesicles before adjusting pH outside of vesicles to 7.4, after adjusting pH and after injecting melittin into vesicles. The vesicles investigated is the ones used in figure 7(a). The vesicles were diluted to 1.5 μM before NTA was performed.

Table 1: Show the raw heat corresponding from injection of different concentrations melittin into 1.5 mM DOPC:DOPS (3:1) pH 9 inside, 7.4 outside vesicles. The different raw heats are integrals of the peaks in figure 7(a).

	100 μM	300 μM	3 mM	6 mM	3 mM in Tris	
Inj nr	Δ Q (μcal)	Δ Q (μcal)	Δ Q (μcal)	Δ Q (μcal)	Δ Q (μcal)	Vol. (μL)
1	-4.7	-3.4	-3.2	-1.7	-0.076	0.400
2	-108.9	-84.6	-54.9	-31.4	-0.88	5.00
3	-103.1	-79.9	-51.6	-27.9	-0.76	5.00
4	-96.4	-75.2	-46.5	-30.1	-0.62	5.00
5	-91.1	-70.7	-39.9	-25.5	-0.61	5.00
6	-85.7	-66.4	-36.2	-23.5	-0.54	5.00
7	-80.3	-62.4	-36.0	-22.5	-0.44	5.00
8	-75.5	-58.8	-34.2	-21.5	-	5.00

4.2.2 α-syn induced vesicle leakage

To investigate whether α-syn had an effect on proton permeability of vesicles, similar to that of melittin, α-syn monomer was injected into vesicles. Figure 9 show the corresponding change in DP from injections of 155 μM monomeric α-syn into 1.5 mM DOPC:DOPS (3:1). Table 2 show the raw heat corresponding

from the injections in figure 9.

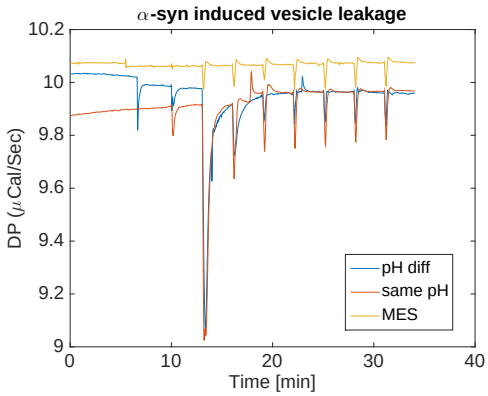

Figure 9: Show the change in heat flux corresponding from injection of α-syn in vesicle solutions. 155 μM α-syn was loaded in the injection syringe and 1.5 mM sonicated DOPC:DOPS (3:1) in the sample cell. An initial injection of 0.4 μL followed by 7 injections of 5μL was performed. In blue; vesicles with pH 6.7 inside and 5.5 outside was used. In orange; vesicles with 5.5 inside and outside was used. In yellow; α-syn was injected into MES pH 5.5. The experiment was performed at 37 °C with 500 RPM stirring in a PEAQ-ITC.

Table 2: Show the raw heat corresponding from injection of α-syn monomer in vesicles with and without a pH gradient between the interior and exterior of the vesicles. The different raw heats are integrals of the peaks in figure 9.

	pH Diff	Same pH	MES	
Inj nr	Δ Q (μcal)	Δ Q (μcal)	Δ Q (μcal)	Vol. (μL)
1	-1.31	-2.09	-0.04	0.400
2	-36.20	-34.82	-0.52	5.00
3	-6.04	-3.51	-0.47	5.00
4	-0.51	-2.00	-0.13	5.00
5	-0.40	-1.85	-0.63	5.00
6	-1.06	-2.29	-0.60	5.00
7	-1.11	-2.12	-0.61	5.00
8	-1.23	-2.00	-0.54	5.00

5 Discussion

The main questions behind this work was whether the spontaneous and seed/vesicle induced aggregation of α-syn was detectable through calorimetry. These questions were prompted by unpublished, preliminary results obtained by Erik Hellstrand, 2012. A second underlying question throughout this work was whether α-syn vesicle co-aggregation would disrupt the vesicle bilayer and cause proton leakage across the membrane. To be able to quantify the extent of protons leaking across the vesicle bilayer, a series of ITC experiments where melittin was injected into vesicles with alternating pH inside and outside vesicles was performed.

5.1 α-syn fibrillation

To investigate the accompanying enthalpy change associated with the fibril formation of α-syn monomer, monomer in the 30 μM range was incubated at 37°C in a VP-ITC. These scans yielded limiting results and as a consequence, scans of monomer with vesicles and seeds present were performed. After a series of experiments yielding vague data of the enthalpy change of the fibrillation process, the concentration of α-syn was significantly increased to 134 μM and a scan with seeds present were performed in a VP-DSC, see figure 1(e), where seven, ≈16.5h consecutive isothermal scans of the same monomer solution was performed. Interestingly the first scan, in blue, showed a different slope than the 6 succeeding scans. Different moving average filters were applied to the data, in an attempt to better elucidate the change in signal and possibly to visualize a peak. The data treatment managed to reduce the signal to noise ratio, but a clear peak was not made distinguishable from what as easily could have been a drift in baseline and due to instrumental detection limits. The filtering period used for this first experiment in the DSC was five seconds. This is the setting for over which time interval raw data is averaged and a data point is stored, for a sharp transition eg. the phase transition of lipids when heated, requires frequent sampling of raw data to resolve the peak of transition. The isothermal aggregation of α-syn is a much slower process, and therefore frequent sampling of the raw data of the process possibly introduce unnecessary noise in the data set. When the filtering period was changed to 25s, figure 1(a)-(d), clear transition peaks were visible for the other scans performed with the same concentration monomer and seed as figure 1(e).

Interestingly, the observed enthalpy change for the processes taking place during the first scan in figure 1(a)-(e) is endothermic. (a common misconception is that a positive peak in a DSC or ITC thermogram is exothermic, this is not the case. When heat is consumed in the sample cell, the heat flux (DP) increases to compensate for the thermal difference between the cells). It is compelling to think that the response of the signal in figure 1(a)-(d) is due to the fibril formation of α-syn. If this is the case, the observed peak in the isothermal scans

in 1(a)-(d) is probably arising from the much more rapid secondary nucleation, than the slower primary nucleation of α-syn monomer. Other processes taking place during the scan, like fragmentation of fibrils and monomer binding to fibrils are also things that influence the overall observed enthalpy change in the scans. Precipitation of insoluble fibrils is also something that might cause bias and artifacts in the measurements, when they presumably falls to the bottom of the sample cell and comes in contact with the cell bottom. This is somthing that is likely to change the heat capacity of the system.

If the process of fibril formation is endothermic under the investigated conditions, it means that the overall process is entropy driven, in the light of the relation $\Delta G = \Delta H - T\Delta S$, where ΔG must be negative for a reaction to occur spontaneously. On one hand one could argue that the reaction is not occurring spontaneously due to the fact that it is catalyzed by pre formed fibrils, and on the other hand one could state that these fibrils would have formed themselves given time. It would have been interesting to perform a longer scan of only monomeric α-syn at the same concentration, to see what the corresponding thermogram would look like in the DSC.

Working with the view that the overall process of fibrillation is endothermic means that the gain in entropy of the system must overcome this positive change in enthalpy, for the process to proceed. The entropy of the protein itself, going from monomeric form to aggregated form is probably decreasing, but the burial of hydrophobic side chains within the fibril cores is something that could increase the system's overall entropy, by increasing the entropy of water (by disrupting the coordination spheres around the hydrophobic parts of the protein).

In the study where mature α-syn fibrils were denatured by thermal up scans performed by DSC [20], the corresponding thermogram exhibited an exothermic peak for the denaturation of the fibrils. The authors further suggests a positive enthalpy change for the formation of α-syn fibrils, something that agrees with the thermograms obtained for the fibril formation observed in this thesis 1(a)-(d). The time for when the peaks occurred is also within the same range as seen in other seeded α-syn kinetic experiments using orthogonal methods (eg. Tht fluorescence in a plate reader [27]).

The spontaneous fibrillation of 39 μM α-syn was monitored in a VP-ITC, see figure 2(a), after $\approx$25h seeds were added to a final concentration of 1 μM see figure 2(b). For the scan in (a) there is no visible peak indicating fibrillation. The filter period used in these scans were two seconds, and from the earlier statement made surrounding the filter period. The fibrillation might not even be distinguishable from the baseline using such a frequent data sampling time constant. If no fibril formation occurred in (a), the peak corresponding from injection of seeds into the solution in (b) gives insights about the enthalpy of binding of monomer to fibril. Another scenario is that the monomer had already fibrillated and the injection peak in (b) is caused by the dilution enthalpy of the

seeds injected.

The scans where seeds were injected into α-syn monomer, were not designed to investigate the associated binding of monomer to fibril, but rather to investigate the fibrillation process. However from the injection peaks where seeds were injected into monomer, the overall tendency of the elongation (monomer binding to fibril) seems to be exothermic. The injection of seeds in figure 3(a) display both an exothermic followed by an endothermic signal. This might be because of a more complex process than only monomer binding to fibril. The endothermic tail of the injection may also have been caused by a small bubble. When performing binding experiments with ITC, usually the injections are initiated with a small first injection to dislodge the potential little air bubble present at the tip of the injection syringe. Figure 10(a) in appendix 1, also contain this similar endothermic tail, when seeds were injected into monomer, but the overall character of the injection peak is exothermic. Figure (b) is a magnification of the scan following the injection of seeds, and although the scan is quite "spiky", a small change in heat capacity of the system is observed $\approx$ 200 minutes after the injection is made and lasting for 250 minutes before the baseline becomes stable. This is within the same range as the peaks observed in figure 1(a)-(d) and could possibly be a consequence of aggregation. The same small divination in the signal is also observable in figure 3(b) between 9 and 14 hours, approximately 9 hours after injection.

In figure 4(a) & (b), 24 μM α-syn were incubated with 0.17 mM DOPC:GM1(9:1) vesicles, same pH inside and outside vesicles, figure (b) bear the resemblance of the peaks obtained in 1(a)-(d), however no distinct baseline is present before the peak starts evolving. This could maybe have been avoided by injecting the vesicles into the monomer solution, once a steady baseline was obtained, rather than having them pre mixed in the sample cell. The scan in (a) displays a peculiar characteristic, maybe due to a dirty cell/syringe, which alters the systems heat capacity. Since (b) did not display the similar tendency the data generated is probably due to some artifact.

When monomer was incubated with SUV's, with a higher pH inside than outside, figure 11(a) & 12(e)-(f) appendix 1., a small exothermic deviation is observed in the baseline after approximately 1000 minutes in both cases. If this change was due to monomer interacting with the bilayer or whether the leakage is caused by the SUV's rearranging themselves, into larger structures, is hard to tell. To further investigate the possible lytic effect of α-syn on vesicles, α-syn monomer were injected into SUV's with and without a pH gradient, figure 9. The area of the injection peaks decreases rapidly with the first injection. There is no significant difference between the area of the peaks were monomer is injected into SUV's with pH gradient than those without. This indicates that significant leakage is not observed. Interestingly though, is the fact that the peaks are decreasing quickly, this could mean that there exist a few preferential binding sites on the vesicles, which gets saturated quickly with the first injec-

tions. Possibly domains of negatively charged lipids or other structural features of the vesicles, size or curvature which promote binding of monomer.

5.2 Melittin induced vesicle leakage

An attempt was made to develop a method for investigating vesicle leakage using ITC. The lytic peptide melittin was injected into vesicle solutions with and without a pH gradient between the interior and exterior of the vesicles. In these experiments Tris was used because of its relatively high ionization enthalpy; $TrisH^+ \rightleftharpoons Tris + H^+$, $\Delta H_{ion} = \pm 47.45 kj \cdot mol^{-1}$ at 298.15 K [28]. The idea behind this method was to inject melittin into a solution of SUV's, and cause leakage of their internal solution. By having a higher pH inside the SUV's than outside, the internal solution would upon leakage be protonated, and the protonation enthalpy measured by ITC.

As expected the observed enthalpy change for injecting melittin into SUV's with a pH gradient was greater than for those without. Something that might interfere with this observation is the possibility that when a pH gradient is present between the interior and exterior of the SUV's the enthalpy of binding of melittin to vesicles might be altered. The negatively charged head-group lipids, DOPS, might have preference for the outer layer of the bilayer, facing the more acidic outer solution [29]. To rule the possibility of this out and to investigate whether this might be a scenario, the experiments could have been performed with vesicles containing only zwitterionic DOPC.

Figure 5 show the injection of 75 μM, 25 μL aliquots melittin into SUV's DOPC:DOPS (3:1). When melittin were injected into 0.5 mM SUV's with a pH gradient (blue data set). The two first injection enthalpies are close to identical. The following injections, result in a gradually decreasing signal. The signal does not decrease to the size of injecting melittin into vesicles without a pH gradient (orange). One reason for not observing full leakage might be because of new melittin injected binds to vesicles which have already leaked. When the SUV concentration was decreased to 0.1 mM, with a pH gradient, the observed DP for injection of melittin was close to that of injecting melittin in SUV's, without a pH gradient and also close to that of injecting melittin in buffer without SUV's. The injection of melittin into the experimental buffer pH 7.4 (violet), and the injection of melittin into buffer pH 9 adjusted to pH 7.4 in the same manner as the SUV solutions, provides insights about how accurate the pH adjustions were. Figure 6(a)&(b) show the size of the vesicles before and after pH adjustment, and after injection of melittin into 0.5 mM and 100 μM vesicle solutions, same vesicles as those in figure 5. The mean size is distributed around 100 nm, in (a) the size of the vesicles are slightly decreased when a pH gradient is introduced. Having a higher concentration H^+ outside the vesicles will probably cause an osmotic pressure and there will be a potential for water to exit the vesicles, and this may explain the shrinkage

of the vesicles. After melittin is injected the size slightly increases again. The trend is not the same in (b), here the size is slightly larger after pH adjustments.

To further investigate the effects of pH gradient on the size of vesicles, experiments focusing solely on the size could be performed. It would have been interesting to perform multiple size determinations at fixed time intervals after sonication, to get a clearer picture on how fast SUV's rearrange themselves into larger structures.

Since full leakage of the SUV's internal solution was not observed after injecting melittin into varying SUV concentrations, the vesicle concentration was fixed and the melittin concentrations varied. Figure 7(a) show the injection of 5 μL melittin aliquots of 100 μM, 300μM, 3 mM, 6mM in 1.5 mM SUV's with a pH gradient. Increasing the melittin concentration was thought to increase the observed leakage, but rather the observed change in DP decreased with an increased melittin concentration. This promoted the idea that melittin might react with itself, this could have been further investigated by injecting melittin into melittin. Another explanation for this behavior is the possibility that protons leaks across the bilayer spontaneously. The same SUV's were used for all the experiments in figure 7(a), starting with injection of 100 μM melittin shortly after sonication and pH adjustment. Approximately one hour passed before the next higher concentration melittin was used. The difference in ionic strength between the interior and exterior of the SUV's might have the potential of causing them to leak, and perhaps the redistribution from smaller size vesicles into larger happened during the experiment. The stirring of the solutions during the ITC experiments might also be something that have the potential of agitating and to cause a size redistribution, leading to bias in the experiments.

The experiment was repeated but instead of increasing the melittin concentration from 100 μM and upwards, the concentration was decreased from 100 μM. Figure 15(a) in appendix 2. Interestingly, the injection of 100 μM melittin in figure 15(a) yielded a much lower observed enthalpy change than the injection of 100 μM melittin in figure 7(a). This might display some of the problems with repeatability in the experimental design. The injections of 100, 50, 25 and 10 μM melittin in figure 15(a) was in the size range of injecting melittin in pure buffer. A different explanation for this might be that the melittin used in figure 15(a) was degraded or aggregated, or the experiment were subject so some other type of contamination.

Figure 17 in appendix 2 show the injection of 7.9 mM melittin into 0.1 mM SUV's (blue), all the melittin is thought to bind to the vesicles, because no decrease in signal is observed. The melittin concentration was doubled and injections were continued into the same SUV's. This caused a gradual decrease in signal, likely from saturation of binding sites on the SUV's.

All the experiments where melittin were injected in SUV's were performed at

37°C. Because the high pH temperature dependence of Tris, and the fact that the pH was adjusted at room temperature is something that has introduced errors throughout the experiments.

6 Conclusions

This work shows that the isothermal seeded fibrillation of α-syn is detectable through calorimetry. Further work would include performing isothermal scans of SUV's incubated with α-syn monomer, using the same instrumental settings as where fibrillation was observed. Introducing a pH gradient between the interior and exterior of the co-incubated SUV's might have the potential to elucidate to which degree the coaggerigation might distrupt the SUV's bilayer.

Groundwork has been laid in the development of a new vesicle leakage assay using ITC. Further work lies in finding a ratio between lytic species and vesicles to a point where full leakage may be observed.

7 Appendix 1

7.1 Additional isothermal scans of α-syn fibrillation

7.1.1 Monitored in PEAQ-ITC

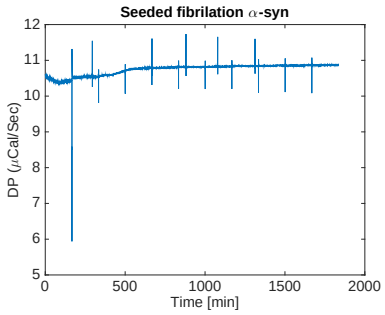

(a)

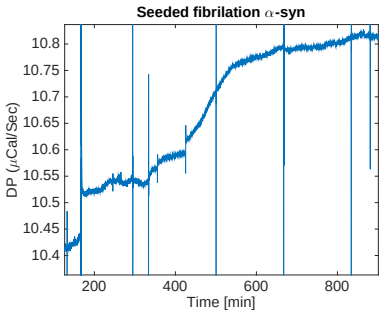

(b) Zoom of (a) after injection of seeds

Figure 10: (a)&(b) Shows the isothermal scan of 28 μM-syn monomer incubated at 37°C and the injection of 20μL 15μM seeds to a final cell seed concentration of 1μM. (b) is a zoom in of the scan after injection of seeds.

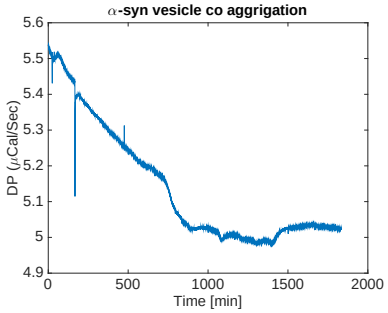

(a) injection of vesicles in monomer

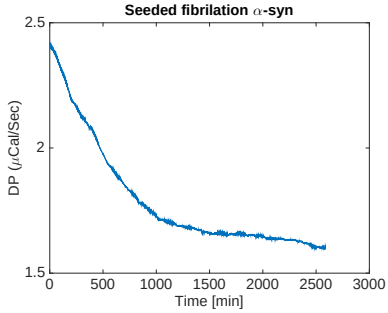

(b) Same sample as used in figure 1(b)

Figure 11: Show isothermal scans performed at 37 °C without stirring in a PEAQ-ITC. In (a) 35 μL, 4.47 mM sonicated DOPC:DOPS (3:1), pH 6.7 inside vesicles, 5.5 outside is injected into the sample cell containing α-syn monomer to a final cell concentration of 0.5 mM vesicles and 25 μM monomer. 0.1 μL injections of vesicles were performed every 2.8 hour. Figure (b) show the scan of the same sample used in 1(b), In the sample cell: 134 μM α-syn monomer, 2 μM seeds. 0.1 μL injections of buffer were performed every 2.8 hour. The buffer used in both runs; 10 mM MES, 0.01 % NaN3 pH 5.5.

7.1.2 Monitored in VP-DSC

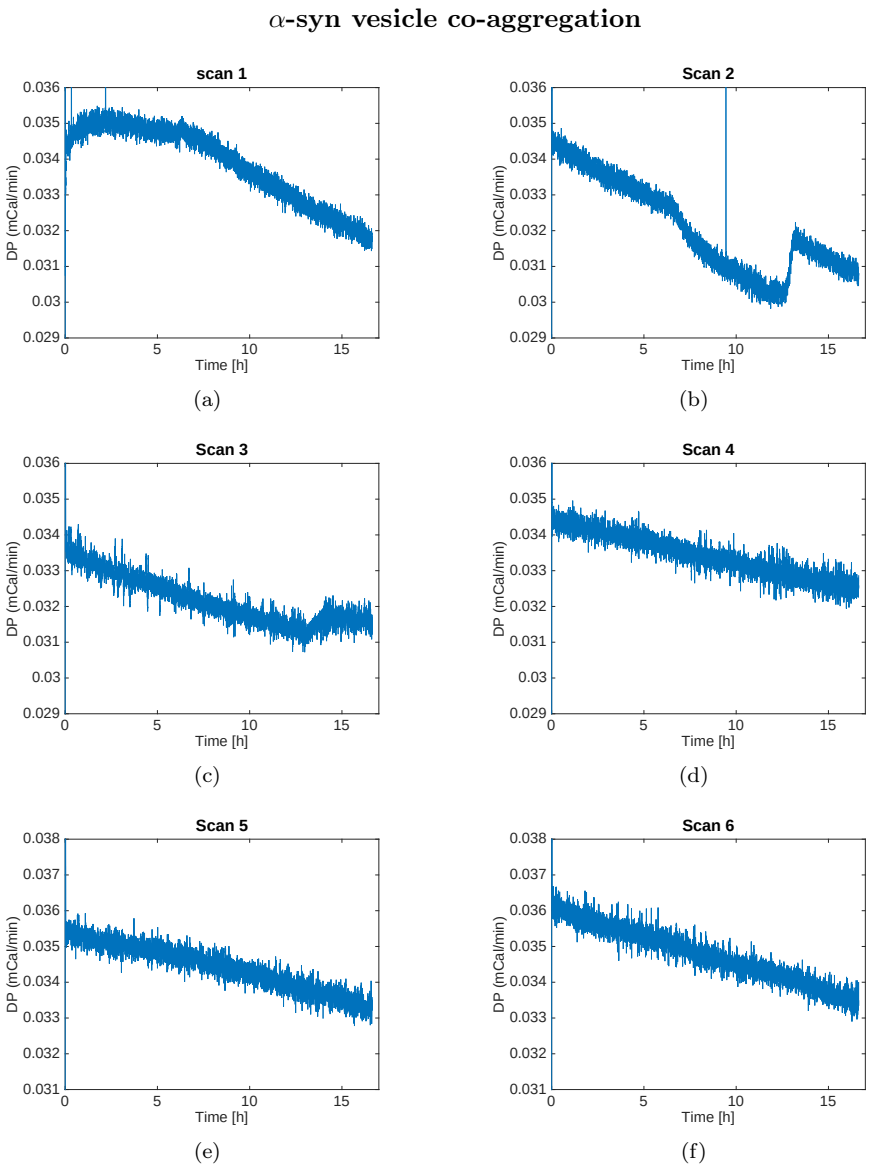

Figure 12: (a-f) shows 6 consecutive isothermal scans, of the same sample. In the sample cell: 24.5 μM α-syn monomer, 0.5 mM sonicated DOPC:DOPS (75%:25%, pH 6.7 inside SUVs, pH 5.5 outside.) in 10 mM MES, pH 5.5. Degassed milli Q water was used in the reference cell. The scans were performed at 37°C, using isothermal scan mode, a filtering period of 5 sec and low feedback mode.The monomer used in the scans had been stored on ice for two days prior to scan nr. 1.

7.1.3 Monitored in VP-ITC

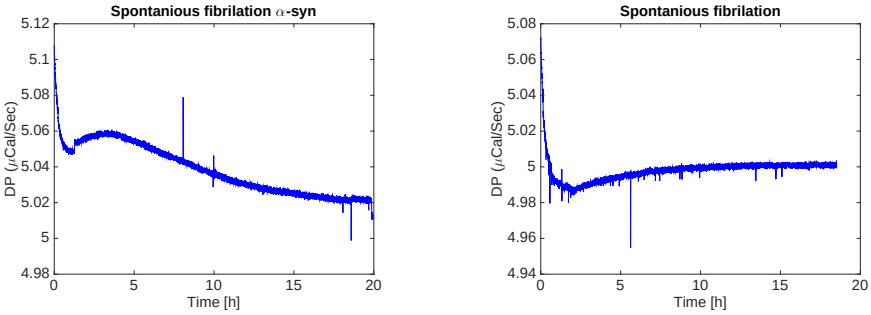

(a) 170202 (b) 170131

Figure 13: (a)&(b) Shows the isothermal scans of 30 μM-syn monomer incubated at 37°C

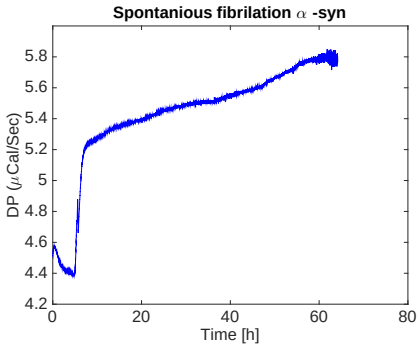

Figure 14: Shows a less optimal scan of 30 μM-syn monomer incubated at 37°C, the cause of the noisy signal could be a trapped air boubble or a dirty cell. This scan show how important proper degassing and sample preparation is.

8 Appendix 2

8.1 Melittin induced vesicle leakage

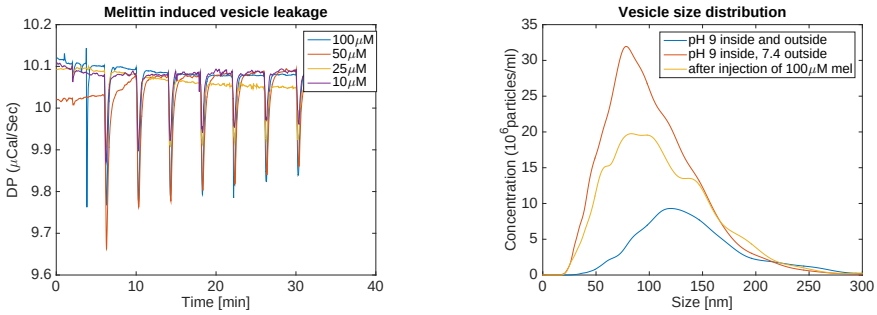

(a) 170202 (b)

Figure 15: (a) Shows the corresponding change in DP from injecting the same volume, 5 μL melittin of different concentrations, into a constant concentration of 1.5 mM DOPC:DOPS (3:1) pH 9 inside, 7.4 outside vesicles. The experiments were performed at 37 °C, 500 RPM stirring in a PEAQ-ITC. (b) shows the size of vesicles before and after pH was adjusted, and after injection of 100 μM melittin.

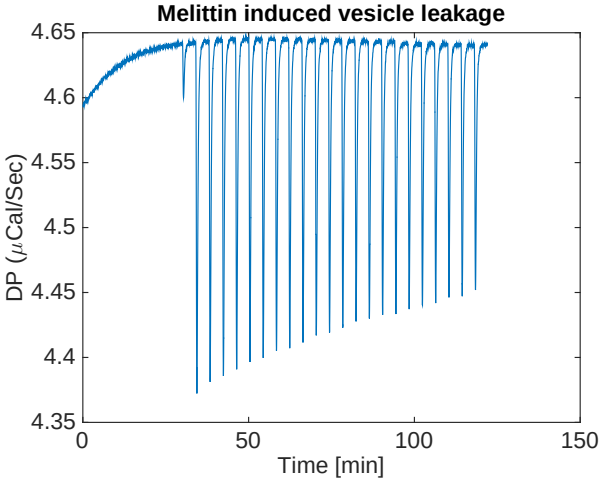

Figure 16: Shows the corresponding change in DP from injecting 12.5μL aliquots, 0.3 mm melittin into 0.5 mM sonicated DOPC:DOPS (3:1) pH 9 inside, 7.4 outside vesicles.The experiment was performed at 37°C,with 307 RPM stirring in a VP-ITC.

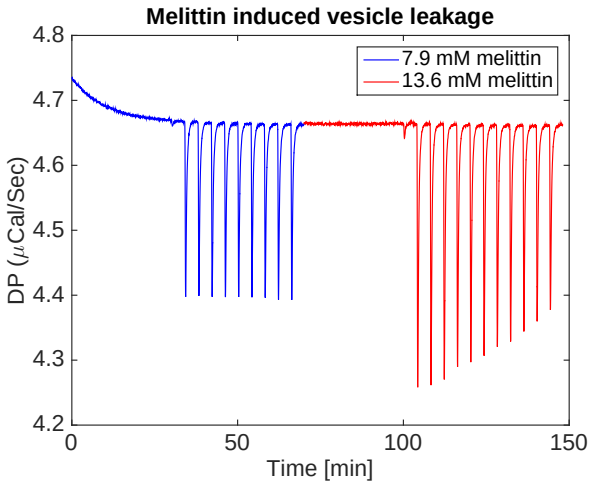

Figure 17: Shows the corresponding change in DP from injecting in blue 7.9 mM melittin, red 13.6 mM melittin into 0.1 mM DOPC:DOPS (3:1) same pH inside and outside vesicles. First 25 μL aliquots of 7.9 mM were injected(blue), after the injections, excess solution was removed from the ITC sample cell. The syringe was reloaded with 13.6 mM melittin and 25 μL aliquots was injected (red) into the same vesicle solution as before. The experiment was performed at 37°C,with 307 RPM stirring in a VP-ITC.

9 Bibliography

References

[1] Richard L Zijdeman and Filipa Ribeiro de Silva. Life expectancy since 1820. *How was Life? Global Well-being since 1820*, pages 101–116, 2014.

[2] Haidong Wang, Mohsen Naghavi, Christine Allen, Ryan M Barber, Zulfiqar A Bhutta, Austin Carter, Daniel C Casey, Fiona J Charlson, Alan Zian Chen, Matthew M Coates, et al. Global, regional, and national life expectancy, all-cause mortality, and cause-specific mortality for 249 causes of death, 1980–2015: a systematic analysis for the global burden of disease study 2015. *The Lancet*, 388(10053):1459–1544, 2016.

[3] Kenneth D Kochanek, Sherry L Murphy, Jiaquan Xu, and Betzaida Tejada-Vera. Deaths: final data for 2014. *National vital statistics reports: from the Centers for Disease Control and Prevention, National Center for Health Statistics, National Vital Statistics System*, 65(4):1, 2016.

[4] Cleusa P Ferri, Martin Prince, Carol Brayne, Henry Brodaty, Laura Fratiglioni, Mary Ganguli, Kathleen Hall, Kazuo Hasegawa, Hugh Hendrie, Yueqin Huang, et al. Global prevalence of dementia: a delphi consensus study. *The lancet*, 366(9503):2112–2117, 2006.

[5] ERl Dorsey, R Constantinescu, JP Thompson, KM Biglan, RG Holloway, K Kieburtz, FJ Marshall, BM Ravina, G Schifitto, A Siderowf, et al. Projected number of people with parkinson disease in the most populous nations, 2005 through 2030. *Neurology*, 68(5):384–386, 2007.

[6] Massimo Stefani and Christopher M Dobson. Protein aggregation and aggregate toxicity: new insights into protein folding, misfolding diseases and biological evolution. *Journal of molecular medicine*, 81(11):678–699, 2003.

[7] Yu Xia, Tsunao Saitoh, Kenji Uéda, Seigo Tanaka, Xiaohua Chen, Makoto Hashimoto, Leigh Hsu, Chris Conrad, Mary Sundsmo, Makoto Yoshimoto, et al. Characterization of the human α-synuclein gene: genomic structure, transcription start site, promoter region and polymorphisms. *Journal of Alzheimer's Disease*, 3(5):485–494, 2001.

[8] T Reid Alderson and John L Markley. Biophysical characterization of α-synuclein and its controversial structure. *Intrinsically disordered proteins*, 1(1):e26255, 2013.

[9] Akihiko Iwai, Eliezer Masliah, Makoto Yoshimoto, Nianfeng Ge, Lisa Flanagan, HA Rohan de Silva, Agnes Kittel, and Tsunao Saitoh. The precursor protein of non-aβ component of alzheimer's disease amyloid is a presynaptic protein of the central nervous system. *Neuron*, 14(2):467–475, 1995.

[10] Leonidas Stefanis. α-synuclein in parkinson's disease. *Cold Spring Harbor perspectives in medicine*, 2(2):a009399, 2012.

[11] W Sean Davidson, Ana Jonas, David F Clayton, and Julia M George. Stabilization of α-synuclein secondary structure upon binding to synthetic membranes. *Journal of Biological Chemistry*, 273(16):9443–9449, 1998.

[12] Igor Dikiy and David Eliezer. Folding and misfolding of alpha-synuclein on membranes. *Biochimica et Biophysica Acta (BBA)-Biomembranes*, 1818(4):1013–1018, 2012.

[13] Katja Pirc and Nataša Poklar Ulrih. α-synuclein interactions with phospholipid model membranes: Key roles for electrostatic interactions and lipid-bilayer structure. *Biochimica et Biophysica Acta (BBA)-Biomembranes*, 1848(10):2002–2012, 2015.

[14] Marie Grey, Sara Linse, Patrik Brundin, and Emma Sparr. Membrane interaction of α-synuclein in different aggregation states. *Biophysical Journal*, 102(3):79a, 2012.

[15] Diane D Murphy, Susan M Rueter, John Q Trojanowski, and Virginia M-Y Lee. Synucleins are developmentally expressed, and α-synuclein regulates the size of the presynaptic vesicular pool in primary hippocampal neurons. *Journal of Neuroscience*, 20(9):3214–3220, 2000.

[16] Luc Maroteaux, James T Campanelli, and Richard H Scheller. Synuclein: a neuron-specific protein localized to the nucleus and presynaptic nerve terminal. *Journal of Neuroscience*, 8(8):2804–2815, 1988.

[17] Jacqueline Burré, Manu Sharma, Theodoros Tsetsenis, Vladimir Buchman, Mark R Etherton, and Thomas C Südhof. α-synuclein promotes snare-complex assembly in vivo and in vitro. *Science*, 329(5999):1663–1667, 2010.

[18] Stephen J Wood, Jette Wypych, Shirley Steavenson, Jean-Claude Louis, Martin Citron, and Anja Leona Biere. Alpha-synuclein fibrillogenesis is nucleation-dependent implications for the pathogenesis of parkinsons disease. *Journal of Biological Chemistry*, 274(28):19509–19512, 1999.

[19] Alexander K Buell, Céline Galvagnion, Ricardo Gaspar, Emma Sparr, Michele Vendruscolo, Tuomas PJ Knowles, Sara Linse, and Christopher M Dobson. Solution conditions determine the relative importance of nucleation and growth processes in α-synuclein aggregation. *Proceedings of the National Academy of Sciences*, 111(21):7671–7676, 2014.

[20] Tatsuya Ikenoue, Young-Ho Lee, József Kardos, Miyu Saiki, Hisashi Yagi, Yasushi Kawata, and Yuji Goto. Cold denaturation of α-synuclein amyloid fibrils. *Angewandte Chemie International Edition*, 53(30):7799–7804, 2014.

[21] Ana I Azuaga, Christopher M Dobson, Pedro L Mateo, and Francisco Conejero-Lara. Unfolding and aggregation during the thermal denaturation of streptokinase. *The FEBS Journal*, 269(16):4121–4133, 2002.

[22] Sergei V Litvinovich, Shelesa A Brew, Shinichi Aota, Steven K Akiyama, Christian Haudenschild, and Kenneth C Ingham. Formation of amyloid-like fibrils by self-association of a partially unfolded fibronectin type iii module. *Journal of molecular biology*, 280(2):245–258, 1998.

[23] Wojciech Dzwolak, Revanur Ravindra, Julia Lendermann, and Roland Winter. Aggregation of bovine insulin probed by dsc/ppc calorimetry and ftir spectroscopy. *Biochemistry*, 42(38):11347–11355, 2003.

[24] Aviad Levin, Thomas O Mason, Lihi Adler-Abramovich, Alexander K Buell, George Meisl, Celine Galvagnion, Yaron Bram, Samuel A Stratford, Christopher M Dobson, Tuomas PJ Knowles, et al. Ostwald's rule of stages governs structural transitions and morphology of dipeptide supramolecular polymers. *Nature communications*, 5, 2014.

[25] Tatsuya Ikenoue, Young-Ho Lee, József Kardos, Hisashi Yagi, Takahisa Ikegami, Hironobu Naiki, and Yuji Goto. Heat of supersaturation-limited amyloid burst directly monitored by isothermal titration calorimetry. *Proceedings of the National Academy of Sciences*, 111(18):6654–6659, 2014.

[26] Marie Grey, Sara Linse, Hanna Nilsson, Patrik Brundin, and Emma Sparr. Membrane interaction of α-synuclein in different aggregation states. *Journal of Parkinson's disease*, 1(4):359–371, 2011.

[27] Ricardo Gaspar, Georg Meisl, Alexander K Buell, Laurence Young, Clemens F Kaminski, Tuomas PJ Knowles, Emma Sparr, and Sara Linse. Secondary nucleation of monomers on fibril surface dominates α-synuclein aggregation and provides autocatalytic amyloid amplification. *Quarterly Reviews of Biophysics*, 50, 2017.

[28] Robert N Goldberg, Nand Kishore, and Rebecca M Lennen. Thermodynamic quantities for the ionization reactions of buffers. *Journal of physical and chemical reference data*, 31(2):231–370, 2002.

[29] Pieter R Cullis, Michael J Hope, Marcel B Bally, Thomas D Madden, Lawrence D Mayer, and David B Fenske. Influence of ph gradients on the transbilayer transport of drugs, lipids, peptides and metal ions into large unilamellar vesicles. *Biochimica et Biophysica Acta (BBA)-Reviews on Biomembranes*, 1331(2):187–211, 1997.